

# A Numerical Model of Crossed Andreev Reflection and Charge Imbalance

J.L. Webb,<sup>1,\*</sup> B.J. Hickey,<sup>1</sup> and G. Burnell<sup>1</sup>

<sup>1</sup>*School of Physics & Astronomy, University of Leeds, Leeds, LS2 9JT UK*

(Dated: June 9, 2019)

We present a numerical model of local and nonlocal transport properties in a lateral spin valve structure consisting of two magnetic electrodes in contact with a third perpendicular superconducting electrode. By considering the transport paths for a single electron incident at the local F/S interface - in terms of probabilities of crossed or local Andreev reflection, elastic cotunneling or quasiparticle transport - we show that this leads to nonlocal charge imbalance. We compare this model with experimental data from an aluminum-permalloy (Al/Py) lateral spin valve geometry device and demonstrate the effectiveness of this simple approach in replicating experimental behavior.

## I. INTRODUCTION

Crossed Andreev reflection (CAR) is a charge transfer process whereby an electron incident at a normal metal or ferromagnet to superconductor junction may enter the superconductor at energies less than the gap energy  $\Delta$  through simultaneous retroreflection of a hole in a spatially separate, nonlocal electrode. Previous work by others has demonstrated this effect experimentally<sup>12</sup> for a nonlocal or lateral spin valve geometry consisting of two separate normal state electrodes incident with a third superconducting electrode, laterally separated on the scale of the BCS coherence length  $\xi_0$ . The effect has been observed as a negative nonlocal voltage and differential resistance detected across the second normal electrode (detector) through which current is applied (the injector)<sup>3</sup>. CAR has attracted considerable recent interest due to the potential to create solid state quantum entanglement via the splitting of a Cooper pair via CAR, demonstrated by recent experimental studies<sup>4,5</sup>.

Previous work has shown that other competing processes also contribute to the nonlocal effect - elastic cotunneling (EC) by which an electron may tunnel nonlocally via an intermediate virtual state in the superconductor and nonlocal charge imbalance (CI), an effect produced through the creation of charge nonequilibrium in the superconducting electrode through quasiparticle injection and diffusion<sup>6</sup>. Both of these processes have been suggested to fully or partially cancel the CAR effect, by producing an equal but opposite contribution in nonlocal voltage, or to dominate over CAR in the regime near  $T_c$  or near the critical field. The use of ferromagnetic electrodes, magnetized parallel(P) or antiparallel(AP), has been suggested and demonstrated as a potential means to separate the spin-dependent CAR and EC effects<sup>7</sup>.

A number of theoretical models have been developed to model the lateral spin valve by taking an analytical approach - either solutions of the Bogoliubov-de Gennes equations, following the method of Blonder, Tinkham and Klapwijk(BTK)<sup>8,9</sup> for Andreev reflection at a single N/S junction, or by solution of the Usadel equations<sup>10,11</sup>. Such studies suffer the deficiency of being untested against experimental data or being unable to simultaneously fully replicate all the nonlocal effects - particularly those due to nonlocal charge imbalance and the negative nonlocal

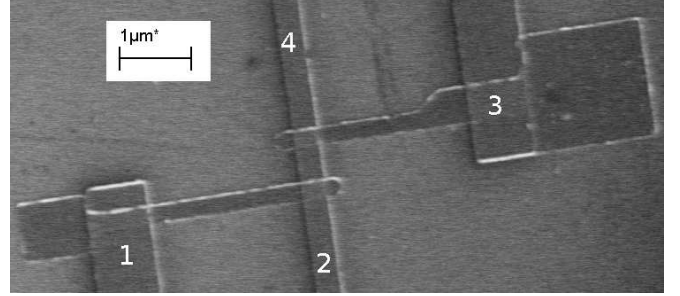


FIG. 1. SEM image of device. Py magnetic electrodes (1) and (3) intersect with an orthogonal Al electrode (2)-(4). Current application and voltage detection is performed as in the text

resistance associated with CAR. In this paper we present a simplified means to model these effects by considering the possibilities for a single electron incident at the local (injector) N/S interface and demonstrate the effectiveness in such an approach in terms of replicating real experimental data.

## II. EXPERIMENT

In order to provide comparison with the model, devices were fabricated for experimental measurement by electron beam lithography using a Raith 50 system in a standard lateral spin valve configuration. These consisted of two Ni:Fe 80:20 (Py) electrodes with  $1 \times 1 \mu\text{m}$  and  $2 \times 2 \mu\text{m}$  nucleation pads and attached nanowire with either a continuous 300nm in width or tapering from 600nm to 300nm (over 400nm), contacting a perpendicular 300nm width Al electrode, of lateral inter-electrode separation 600-900nm (Fig. 1). Patterning was performed using standard PMMA positive resist. Deposition of Py was performed by DC magnetron sputtering at 34W/2.5mTorr Ar at system base pressure  $3 \times 10^{-9}$  torr. Overlay of the Al electrode was by mix-and-match EBL patterning followed by Al deposition at 50W/2.5mTorr Ar at base pressure  $3.2 \times 10^{-8}$  torr, preceded by an in-situ 40s  $\text{Ar}^+$  mill at 410V acceleration voltage to clean the Py electrode surface of oxide and residual resist. Measurement was undertaken in an adiabatic demagnetization refrigerator cooled to 600mK with current injection and local voltage detection between 1-2 in Fig. 1 and nonlocal voltage

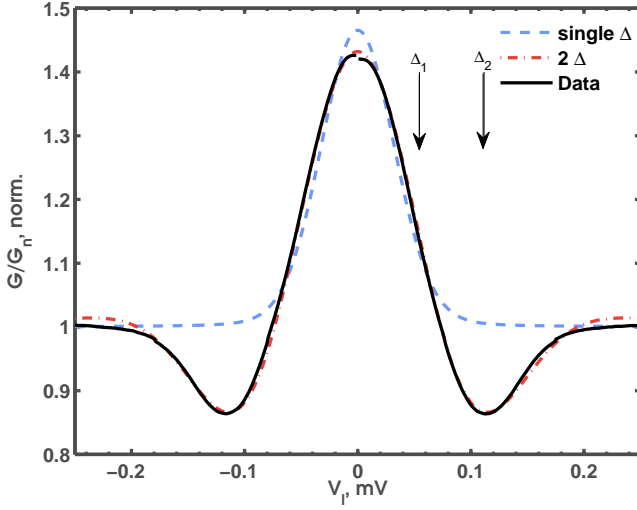


FIG. 2. Local normalized differential conductance  $G/G_n$  for an example injector junction, with BTK model fits using a single- $\Delta$  ( $\Delta_1$ ) and by a two- $\Delta$  ( $\Delta_1$  and  $\Delta_2$ ) method. Fitting parameters of  $P=0.182$ ,  $\Delta_1=0.1491\text{meV}$ ,  $\Delta_2=0.2892\text{meV}$ ,  $Z=0.145$  and  $T^*=1.7\text{K}$  were used, the position of the  $\Delta_1$  and  $\Delta_2$  indicated on the figure.

detection 3-4, using both a DC applied current  $I_{dc} < 100\mu\text{A}$  and nanovoltmeter and AC current  $I_{ac}=0.25\mu\text{A}$  with DC offset  $I_{dc}$  in order to measure differential conductance via a standard lock-in amplifier technique. Low AC frequency of 9.99Hz was used to minimize inductively generated nonlocal voltage observed.

#### A. Local Effect

Differential conductance through the local (injector) junction was measured using the lock-in method with  $I_{ac}=0.25\mu\text{A}$  and DC offset  $I_{dc}$  to  $50\mu\text{A}$ . The resulting data can be seen in Figure 2 and exhibited a subgap enhancement of conductance consistent with single junction Andreev reflection<sup>12</sup>. The model of Blonder, Tinkham and Klapwijk (BTK) and as modified by Strijkers et. al.<sup>813</sup> was fitted to the experimental data by a standard  $\chi$ -squared minimization process to obtain parameters (see figure caption) including spin polarization  $P$ , interface parameter  $Z$  and effective temperature  $T^*$  that were within physical limits. Two methods of fitting were used: with a single gap parameter  $\Delta_1$  and two parameters  $\Delta_1$  representing a region of suppressed superconductivity and  $\Delta_2$ , a higher (bulk) value. Although the single- $\Delta$  approach was capable of replication of the peak at zero and of high  $I_{dc}$  behavior, only the two- $\Delta$  approach was able to replicate the finite bias minima observed at  $I_{dc}=10\text{-}30\mu\text{A}$  in the conductance data. This implied the existence of a region of suppression of the superconductivity in the Al - or a proximity effect induced superconducting region in the injector electrode - potentially arising from the effect of the adjacent magnetic electrode. The low value of  $P$  compared to the  $P=0.3\text{-}0.4$  range expected can be attributed

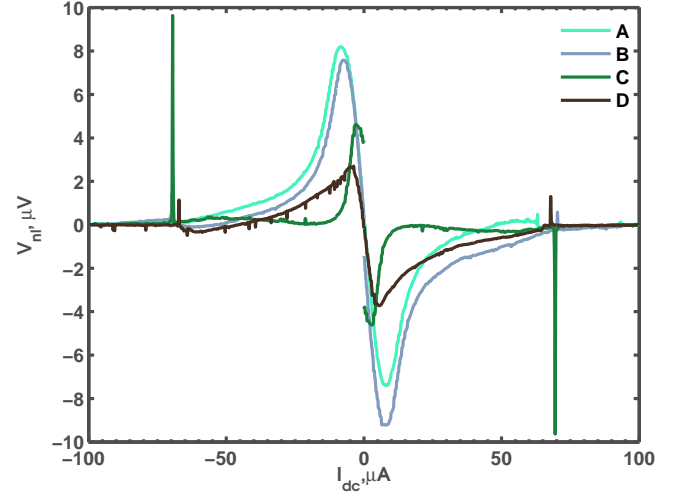


FIG. 3. Nonlocal DC voltage  $V_{nl}$  vs.  $I_{dc}$  at 600mK for 4 devices A, B, C, D of inter-electrode separation  $A=250\text{nm}$ ,  $B=150\text{nm}$ ,  $C=600\text{nm}$ ,  $D=900\text{nm}$

to the non-point contact nature of the junction and that the polarisation returned reflects the effective polarisation at the junction rather than the bulk value for the Py.

#### B. Nonlocal Effect

Examples of nonlocal measurement data taken for a range of devices can be seen in Figures 3-6. Figure 3 shows the nonlocal DC voltage  $V_{nl}$  measured for a range of devices A-D of inter-electrode separation  $L$  250-900nm measured as a function of applied DC current through the injector  $I_{dc}$ . A negative nonlocal voltage was observed, with a general trend of reduction in amplitude with increasing inter-electrode separation  $L$  characteristic of a CAR effect decaying over  $\xi_0$ . This effect can also be seen in a plot of nonlocal differential resistance  $dR_{nl}$  in Figs 4 for two of the devices A, D demonstrating a characteristic shape of finite bias negative minima and zero  $I_{dc}$  peak, attributed to EC and CAR-dominated transport regimes<sup>1415</sup>. The effect was observed to be stable on repetition and highly dependent on the injector/detector selection, reversing the choice producing a lower  $dR_{nl}$  effect likely arising from variation in local junction properties of the injector. The absence of a finite  $dR_{nl}$  at high  $I_{dc}$  was potentially due to the elimination of nonlocal CI effects at the 600mK measurement temperature that would otherwise contribute a finite nonlocal voltage.

#### C. Temperature Dependence

Figure 5 shows the effect of changing temperature on  $dR_{nl}$  vs.  $I_{dc}$  for a separate device  $L=600\text{nm}$ . No effect was observed above  $T_c$  (at  $T>1.3\text{K}$  in the figure). A reduction in both peak height and negative minima depth was observed, due to reduction in nonlocal superconducting effects. A

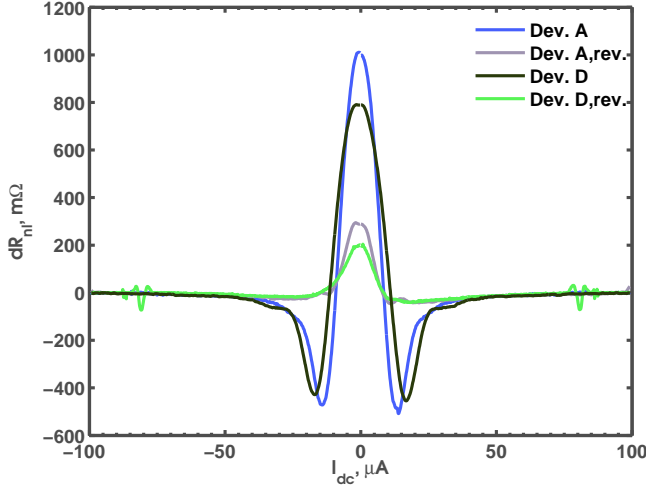


FIG. 4. Nonlocal resistance  $dR_{nl}$  measured via the lock-in technique as a function of  $I_{dc}$  at the injector for device A of inter-electrode separation 250nm and Device D of inter-electrode separation 900nm. Measurements are shown for both configurations of injector/detector; the reverse (*rev*) configuration refers to current injection through the untapered (300nm width) electrode

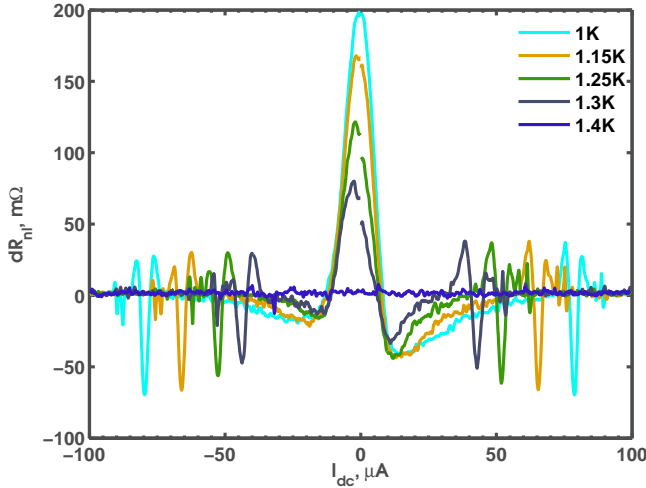


FIG. 5. Al/Py device nonlocal resistance  $dR_{nl}$  as a function of  $I_{dc}$  at a range of temperatures. No signal was detected at  $T \geq 1.4K$ , with  $T_c$  for the device reached at  $\approx 1.35K$ . The asymmetry in  $\pm I$  was a product of the measurement method

shift towards  $I_{dc}=0$  of the zero bias minima was observed, likely due to reduction in  $\Delta$  with increasing  $T$ . At higher  $I_{dc}$  sharp inversions in  $dR_{nl}$  were observed, the position of which reduced in  $I_{dc}$  as temperature increased. We attribute these features to nonlocal charge imbalance, given the temperature and current dependence and similarity in shape to features observed by others- notably in the the work by Cadden-Zimansky and Chandrasekhar<sup>16</sup>.

Figure 6 shows the variation in zero bias ( $I_{dc}=0$ ) peak with temperature from 0.45-1.5K for a separate device. A finite, temperature independent effect was observed as  $T \rightarrow 0$  which

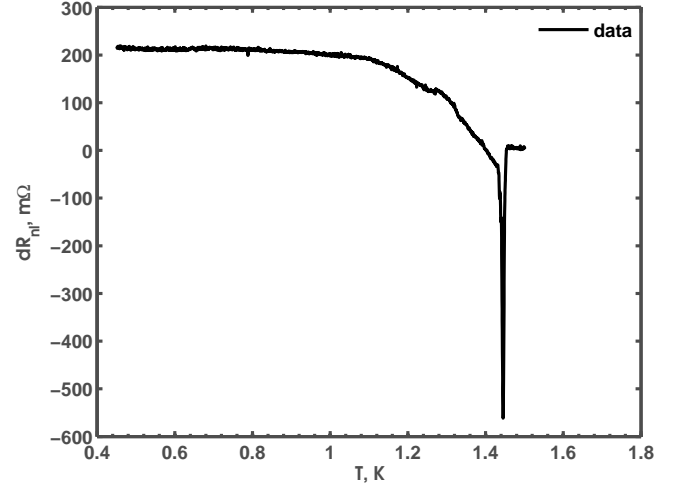


FIG. 6. Experimental temperature dependence of nonlocal differential resistance  $dR_{nl}$  for a separate Al/Py device of slightly higher  $T_c \approx 1.4K$

we attribute to the elimination of nonlocal charge imbalance due to the reduction in the charge imbalance length  $\Lambda_Q = \sqrt{D\tau_Q}$ , with  $D$  the metal diffusion constant and  $\tau_Q$  the charge imbalance time given by:

$$\tau_Q = \frac{4k_B T}{\pi \Delta(T)} \tau_{in} \quad (1)$$

with  $\tau_{in}$  the inelastic scattering time.

At low temperatures, the CI effect is minimized, implying the existence of other non-CI effects (i.e. - EC or CAR) to create the finite peak. As  $T \rightarrow T_c$ , this finite value is reduced to zero with a large inversion in  $dR_{nl}$  close to  $T_c$ . No effect was observed above  $T_c$ , as expected if the measurements were attributable to nonequilibrium superconducting processes. We attribute this inversion effect also to nonlocal charge imbalance, arising from the divergent increase in  $\Lambda_Q$ . Such an inversion effect has been seen in studies of local and nonlocal CI effects<sup>17,18</sup>. Previous works by Beckmann et al.<sup>1</sup> and Kleine et al.<sup>18</sup> have however shown a different form for temperature dependence at zero bias, an increase from a low or zero nonlocal resistance at low temperature to a finite positive peak as  $T \rightarrow T_c$ , followed by a sharp drop to zero above  $T_c$ . We attribute the difference in this work to be due to the presence of an additional finite effect at low temperature, observed as a peak at zero bias and likely arising from EC, and to a differing negative contribution to nonlocal resistance arising from nonlocal CI.

### III. MODELING

In order to understand the experimental effects seen here and elsewhere in the literature, we consider a numerical model of the processes undertaken by a single electron incident at the injector. We initially model the incident electron as a single

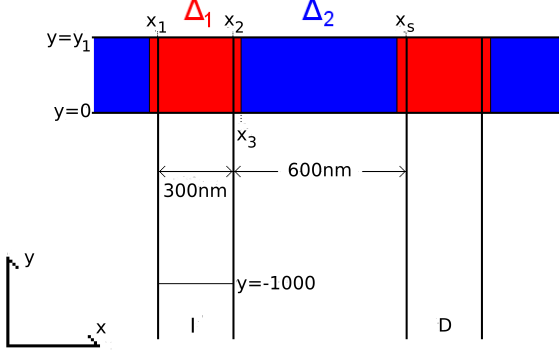


FIG. 7. Schematic of model configuration for a lateral spin valve geometry, with injector (I) and detector (D) electrodes indicated and inter-electrode separation  $L=600\text{nm}$

charge packet, undergoing a random walk diffusive motion in  $\pm x$  and  $\pm y$  (Fig. 7) of step size  $\lambda_F$ , the mean free path in the injector material. Two probabilities  $p_1$  and  $p_2$  are defined such that the likelihood of a move in  $+x$ ,  $P(+x)=p_1$ ,  $P(-x)=1-p_1$  and similarly for  $P(+y)=p_2$ ,  $P(-y)=1-p_2$ . For  $p_1=p_2=0.5$ , the electron may move freely in any direction. By introducing a probability bias, such that for  $p_1 > 0.5$ ,  $p_2 > 0.5$ , a directional preference can be introduced into the motion, replicating the effect of a potential bias. An initial position for the electron is defined at  $y=-1000\lambda_F$  defining the inter-metallic interface at  $y=y_0=0$ . We define positions  $x_1$  and  $x_2$  as the left and right-hand edges of the injector electrode and  $y_1$  the width of the orthogonal electrode, such that for  $y < 0$  the electron is confined within  $x_1$  to  $x_2$ . For  $p_1=0$ , the electron must move within  $\lambda$  of  $x_1$  the left hand edge (i.e. in  $-x$  alone). The directional preference permits replication of the current transport in a real device, that would be confined by the potential to the left-hand  $x_1$  edge.

### A. Normal State

In the normal state, an electron incident at  $y=0$  is free to continue diffusive motion in the perpendicular electrode, with step size equal to the new mean free path  $\lambda_S$  in the material. We define a position  $|x_{lim}|$  whereby the electron is considered to have fully escaped the injector electrodes such that it may pass into the right or left hand side of the perpendicular electrode. For  $-x_{lim}$  (to the left in Fig. 7) this electron is considered to contribute to the local conductance; for  $+x_{lim}$  the nonlocal. An electron exiting to the left is modeled to add  $+1$  arbitrary conductance unit to the local total  $\theta_l$  and exiting to the right adding  $+1$  to the nonlocal total  $\theta_r$ . For  $N_T$  single electrons passed through the system, the total conductance is defined as  $g_l = \sum_N \theta_l$  and similarly for  $g_r = \sum_N \theta_r$ . For  $p_1=0.5$ , the average  $g_l \approx g_r$ , representing an equal chance of electron conductance nonlocally or locally. By experimental measurement of the precise ratio of the voltage generated locally  $V_l$  to that nonlocally  $V_{nl}$  by an applied

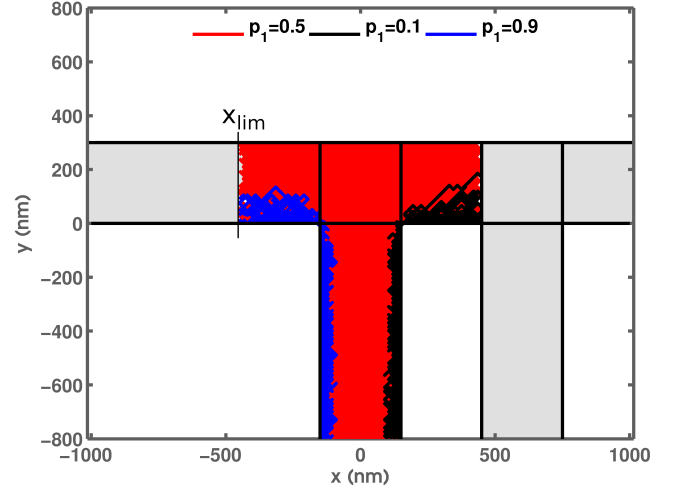


FIG. 8. Map of electron diffusion paths in a device of inter-electrode separation  $L=300\text{nm}$  (for  $N_T=100$ ) in  $x$ ,  $y$  and the normal state (4.2K) at zero injector bias for  $p_1=0.1$  and  $0.9$ , representing the two local and nonlocal transport extremes and the  $p_1=0.5$  case, for equal probability of transport in  $\pm x$ . Here  $|x_{lim}|=450\text{nm}$ , such that an electron may exit the system only when reaching the detector electrode

Process	$\theta_l$ , Local	$\theta_r$ , Nonlocal
AR	$+2$	$0$
CAR	$+1$	$+1$
EC	$+1$	$-1$
Normal reflection	$-1$	$0$
Quasiparticle(CI)	$+1$	$\pm A_Q e^{-x_s/\Lambda_Q}$

TABLE I. Single-electron contributions from each process to local and nonlocal conductance with zero spin polarization  $P_m$ . At the nonlocal electrode CAR is defined to make a positive contribution (exhibited as a negative nonlocal resistance) and EC a negative one

injector current, where  $V_l/V_{nl} \propto g_l/g_r$ ,  $p_1$  can be found giving a precise quantification of nonlocal diffusive current flow in the normal state.

Figure 8 shows the paths taken by  $N=100$  electrons for values of  $p_1=0.1$ ,  $0.5$  and  $0.9$  and  $|x_{lim}|=450\text{nm}$ , illustrating the operation of the model in the normal state. In the case of  $p_1=0.1$  the majority of conduction is nonlocal, indicated by the tracks towards  $+x$  (right), and for  $p_1=0.9$  the majority is local, the paths confined to the inner left edge of the injector in the  $-x$  direction. In the intermediate case,  $p_1=0.5$ , electron diffusion can occur with equal probability in either direction, yielding  $g_l=g_r$ .

### B. Superconducting State

We next consider the superconducting state by introducing two spatially variant values of the superconducting gap  $\Delta_1(x,y)$  and  $\Delta_2(x,y)$  representing a suppressed and bulk energy gap, such that  $\Delta_2(x,y) > \Delta_1(x,y)$ . This follows the

approach of Strijkers et al.<sup>13</sup> considering a proximitized layer of lower- $\Delta$  at the normal-superconductor interface. For the model,  $\Delta_1=\Delta_2=0$  for  $y<0$  in the normal state electrodes. We restrict the spatial extent of the suppressed  $\Delta_1$  to around the region of overlap between the normal electrodes and superconducting electrode for  $0<y<y_1$  and  $|x_3|$  with  $\Delta_2$  covering the remainder of the superconducting region, such that an electron may progress as a quasiparticle excitation in the  $\Delta_1$  region for  $\Delta_1 < E < \Delta_2$  but not into the bulk  $\Delta_2$  region. This is illustrated in Fig. 7. Each electron is defined as possessing an energy  $E$ , taken at random from a Fermi distribution  $f(E-V) = 1/(e^{(E-V)/k_B T} + 1)$  as  $E = -2k_B \ln(f_p)$  where  $f_p$  is a pseudo-random value (0..1),  $V$  the simulated potential across the injector and  $T$  the simulated temperature.

For an electron diffusively entering the region of nonzero  $\Delta$  and  $E < \Delta_1$ , only transmission by Andreev reflection is possible. The probability for AR  $P_{AR}$  is calculated from expressions given by from the model of BTK<sup>8</sup> and the modification by Strijkers. We consider that a fraction of this Andreev reflection may occur as CAR such that  $P_{CAR} = cP_{AR}$  and that a fraction of the current which is not transmitted by AR could be by EC such that  $P_{EC} = c_t(1 - P_{AR} + P_{CAR})$  defining a probability conservation relation  $P_{AR} + P_{CAR} + P_{NR} + P_{EC} = 1$  including the probability of normal reflection  $P_{NR}$ . The factors  $c$  and  $c_t$  defining the CAR and EC fractions are assumed invariant with electron energy or applied simulated potential  $V$ . For each modeled electron, the process undertaken is selected using a pseudo-random value  $p_3 = (0..1)$ , the range to 1 subdivided according to the ratios of probabilities for each process. An electron undertaking any of the processes is said to have exited the system, in a manner similar to that of diffusive exit past  $|x_{lim}|$  - the contributions  $\theta_{r/i}$  for each process are given in Table I.

For  $\Delta_1 < E < \Delta_2$  the electron may still Andreev reflect, cotunnel or may now enter the superconducting electrode as a quasiparticle. We consider the quasiparticle state to be electron-like and modeled as before by diffusive motion - but limited to the  $\Delta_1$  region within  $|x_3|$ , quasiparticle transport into the bulk  $\Delta_2$  region outside prohibited. For  $E > \Delta_2$  this restriction is removed permitting quasiparticle diffusion throughout the superconducting electrode (whilst prohibiting any Andreev reflection). A quasiparticle reaching  $|x_{lim}|$  contributes to the local and nonlocal conductance according to Table I with an exponential decay depending on the separation between the point of exit and the nonlocal electrode  $x_s$ , and decay scale  $\Lambda_Q$  the charge imbalance length. This represents a phenomenological replication of nonlocal charge imbalance, of either negative or positive contribution to the nonlocal effect. The same dependence on inter-electrode separation is introduced for EC and CAR by reducing their fraction of the AR and non-AR probability at the injector according to an exponential form  $c = c_0 e^{-x_s/\xi_0}$  and  $c_t = c_{t0} e^{-x_s/\xi_0}$  on a decay scale equal to the BCS coherence length  $\xi_0$ ,  $c_0$  and  $c_t$  are defined at zero separation (i.e. - at the injector). Since  $E$  is taken from a Fermi distribution, even for low  $V$  all processes are possible at finite  $T$ . The spatial variation in  $\Delta$  permits the control over the width of the gap suppression region,

the continuum of values permitting replication, the proximity effect and potential normal state regions of  $\Delta=0$ . Such a case would permit electron diffusion nonlocally even at  $T < T_c$ .

### C. Spin Dependence

Finally, we consider the case for a ferromagnetic injector and detector electrode by considering a total pool of available electrons of each spin type:  $N_{1\uparrow}, N_{1\downarrow}$  at the injector and  $N_{2\uparrow}, N_{2\downarrow}$ , such that the total number of simulated injected electrons  $N_T = N_{1\uparrow} + N_{1\downarrow}$  and defining the polarisation for the spin in the model  $P_m$  at the injector electrode:

$$P_m = \frac{(N_{1\uparrow} - N_{1\downarrow})}{(N_{1\uparrow} + N_{1\downarrow})} \quad (2)$$

$P_m$  is assumed to be uniform for both injector and detector and represents a means of replicating the bulk spin polarization  $P$  in the ferromagnetic electrode. A simulated electron is selected at random from one of the spin type pools ( $N_{1(\uparrow/\downarrow)}$ ). For  $P_m=0$  this has no effect on the conductance totals or probabilities for any effect. For finite  $P_m$ , such that  $N_{1\uparrow} \neq N_{1\downarrow}$  and  $N_{2\uparrow} \neq N_{2\downarrow}$ , one pool will be exhausted before the other, prohibiting the spin dependent processes (such as AR, CAR) from occurring. For example, in the half metallic case where  $N_{1\uparrow} = N_{2\uparrow} = 0$ , CAR would be prohibited due to the absence of the pairing spin- $\uparrow$  required to form a Cooper pair. This method also permits simulation of magnetization dependence by introducing an imbalance in the spin dependent pools such that  $N_{1\uparrow} > N_{1\downarrow}$  and  $N_{2\uparrow} < N_{2\downarrow}$  in the antiparallel configuration and the reverse for parallel magnetization. The model neglects spin accumulation and the non-local spin valve effect by choice, although such an effect could potentially be included.

### D. Model Examples

Figures 9-11 show the effects on the modeled nonlocal differential resistance  $g_r^{-1}$  for an arbitrary selection of realistic parameters ( $\xi_0=600\text{nm}$ ,  $\Lambda_Q=1\mu\text{m}$ ,  $\Delta_1=0.2\text{meV}$ ,  $\Delta_2=0.4\text{meV}$ ,  $T=600\text{mK}$ ,  $T_c=1.4\text{K}$ ) as a function of inter electrode separation and of temperature for  $N_T=10000$  electrons, both following qualitative trends observed by others<sup>18,15</sup>. Figure 10 can be compared directly to Figure 5 from experiment, the same qualitative trend of reduction in peak and negative minima observed from the model.

Figure 11 shows the temperature dependence at  $V=0$  ( $I_{dc}=0$ ) for 3 configurations - no CI ( $A_q=0$ ) and finite CAR/EC  $c=c_t=0.2$  and with CI switched on:  $A_q=1$  with absence/presence of CAR/EC. We model CI as a negative contribution to the nonlocal resistance  $g_r^{-1}$  to assist replication of the effects observed experimentally. In the case of CI-only, no finite effect is seen at low- $T$ . This did not match the result for the real Al device in Fig. 6 which qualitatively follows the model form with finite-CAR/EC contribution as  $T \rightarrow 0$  and CI divergence as  $T \rightarrow T_c$ . Divergent behavior is replicated as  $T \rightarrow T_c$ , the case for finite CI and finite EC/CAR best - but

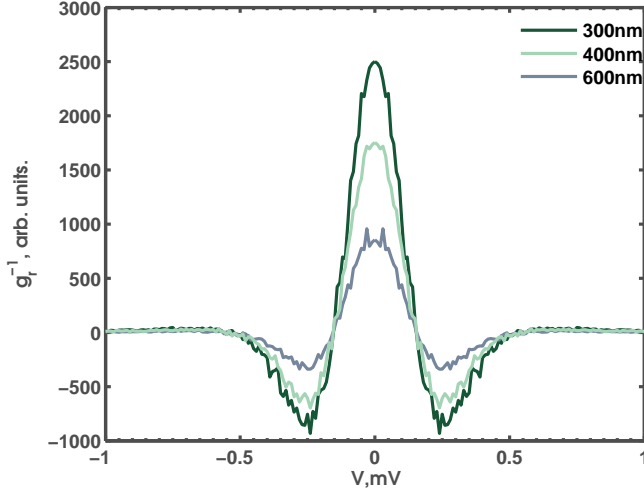


FIG. 9. Example of model output I: nonlocal differential resistance  $g_r^{-1}$  as a function of  $V$  for inter-electrode separation  $L=300-900\text{nm}$

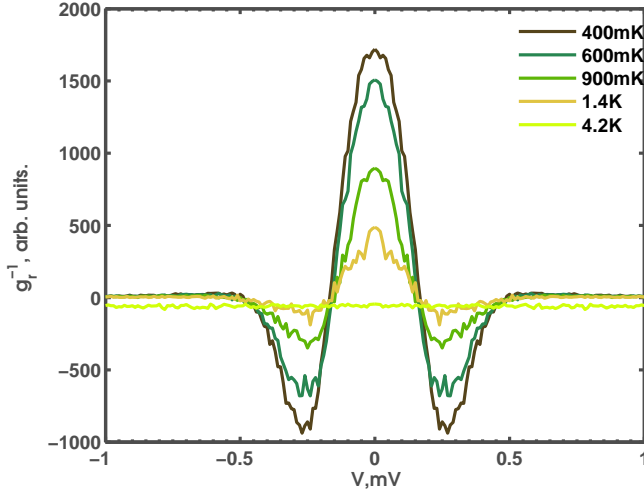


FIG. 10. Example of model output II: differential resistance  $g_r^{-1}$  vs.  $V$  at a range of temperatures  $T=400\text{mK}-4.2\text{K}$ , with  $A_q=0$  and parameters as in the main text

not precisely - replicating the observed experimental trend. The CI effect was considered to produce a negative effect - if a positive effect was instead considered, the behavior for  $A_q=1$ ,  $c=c_t=0$  (CI only) replicates the observed behavior seen by others<sup>1861</sup> as an increase to a finite peak from low- $T$  zero  $g_r^{-1}$  with zero effect above  $T_c$ .

### E. Match to Experiment

In order to demonstrate the capability of the model, the transport behavior of the real device was compared to the model result from inputting parameters realistic for the fabricated devices. The result of this is shown in Figure 12 giving the model result overlaid onto real nonlocal differential

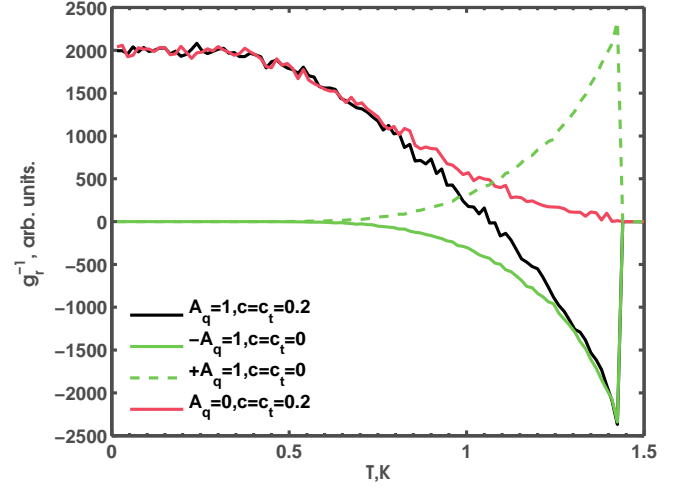


FIG. 11. Example of model output III: T-dependence for absence/presence of charge imbalance  $A_q=0/1$  and absence/presence of EC/CAR ( $c, c_t$  values) at  $V=0$ . The result for negative CI contribution ( $-A_q$ , solid) is shown with the mirrored result for positive contribution ( $+A_q$ , dashed)

resistance data from experiment. Model parameters were selected to best represent the device or from measurement of device properties. Parameters  $x_1=-150\text{nm}$ ,  $x_2=+150\text{nm}$  (giving width= $300\text{nm}$ ) were fixed based on the physical dimensions of the device. The point of diffusive exit from the system  $|x_{lim}|=450\text{nm}$ , taken as the half-way point to the detector electrode with inter-electrode separation  $L=600\text{nm}$ , based on the assumption arrived at through simulation that the majority of electrons crossing past  $x=300\text{nm}$  would follow a trajectory reaching the second electrode at  $x=750\text{nm}$ .  $|x_{lim}|$  was also minimized to reduce computation time, but to be sufficiently high to inhibit premature exit of the electron from the system.

Values of  $\lambda_s=15\text{nm}$ ,  $\lambda_F=5\text{nm}$  and  $\Lambda_Q=1\mu\text{m}$  were used, based on physically reasonable parameters from previous work for nonlocal spin value devices and on nonlocal charge imbalance.  $\xi_0=500\text{nm}$  was taken, assuming a relatively clean superconducting Al electrode, but with a degree of suppression of the coherence length from the BCS value and sufficiently long to produce non-negligible superconducting nonlocal effects over the inter-electrode separation used. Although a value was set for  $\Lambda_Q$ , based on the temperature independence of the nonlocal effect at the  $600\text{mK}$  experimental measurement temperature (Fig. 6) the assumption was made of complete suppression of nonlocal charge imbalance, introduced into the model by setting  $A_q=0$ . This was based on the hypothesis from experimental data that the origin of the nonlocal effect at  $T \ll T_c$  was from processes operating over a decay scale  $\xi_0$  (i.e. - CAR/EC) rather than CI. This assumption would not be valid for  $T \rightarrow T_c$ , where additional CI effects would arise from the divergence of  $\Lambda_Q$  and cannot replicate the temperature dependent effect observed experimentally.

Modeled  $T_c$  was set to  $1.4\text{K}$ , close to that observed in



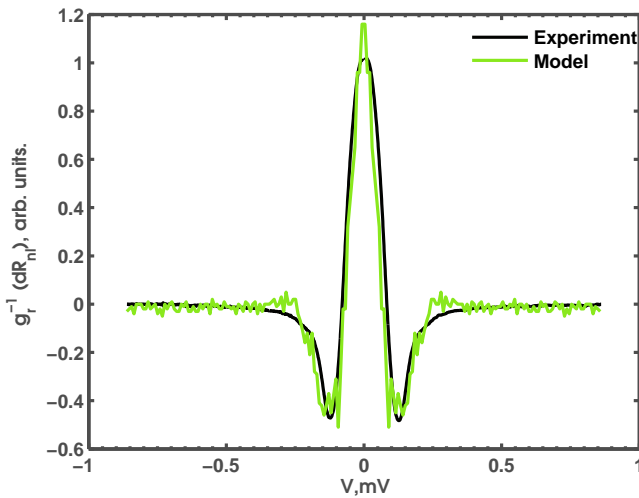


FIG. 12. Nonlocal differential resistance as a function of applied injector DC current  $I_{dc}$  for modeled and experimental data

experimental data. Using this value of  $T_c$ , we calculated physically reasonable values for  $\Delta_1(T=600\text{mK})=0.056\text{meV}$ ,  $\Delta_2(T=600\text{mK})=0.15\text{meV}$  derived from standard BCS theory and fits to local conductance data. The ratio of bulk to suppressed  $\Delta$  was taken based on the width of the negative minima from the experimental data, making the assumption that the suppressed  $\Delta_1$  represented approximately the low- $I_{dc}$  zero crossing (at  $\approx 10\mu\text{A}$  on Fig. 4) and bulk  $\Delta_2$  the higher  $I_{dc}$  return to zero (at  $\approx 30\mu\text{A}$ ), a ratio of approximately 1/3. We base the requirement for the two values of  $\Delta$  on the local experimental data, whereby a region of lower energy gap was required to correctly fit the conductance behavior - this region likely being that immediately adjacent to the magnetic electrodes. On this basis we limit the  $\Delta_1$  region extent  $|x_3|$  to within the overlap region of the injector/detector electrodes  $-150 < x < 150$ . We neglect any proximity effect into the injector, confining the superconducting region of nonzero  $\Delta$  strictly to within the perpendicular lateral electrode for  $300 < y < 0$ .

The values of  $c$  and  $c_t$  represented free parameters which were selected to give the best fit to the experimental data, each parameter effectively controlling negative minima depth and zero bias peak height of nonlocal resistance  $g_r^{-1}$  respectively. We make the assumption that both  $c$  and  $c_t$  are invariant with other parameters such as  $T$  or injector bias. Values of  $c=0.28$  and  $c_t=0.15$  were found to give a best fit, implying the presence of both effects but an imbalance in a 2:1 ratio between them such as not to cancel each other, with each

producing a different effect at varying simulated bias.

In order to translate the arbitrary conductance units used in the model to real nonlocal resistance (in Ohms) the conversion  $g_r=k\delta R_{nl}$  was used with  $k$  a scaling factor of 1000. A total of  $N_T=10000$  electrons were simulated for each step in simulated injector  $V$  using  $p_1=0.555$  to account for the nonuniform distribution of current arriving at the injector, even in the superconducting state. A good fit was found to the experimental conductance data as can be seen in the figure, the only discrepancies arising in the height of the peak, potentially due to a slightly high values of  $c$  or  $c_t$  and a discontinuity around  $0.23\text{-}0.3\text{mV}$  due to the  $2\text{-}\Delta$  approach taken, rather than a continuous range of  $\Delta$  arising from the proximity effect. The fit was obtained with no nonlocal charge imbalance included ( $A_q=0$ ), supporting the idea of the absence of such effects at low temperature.

#### IV. CONCLUSION

In conclusion, we have fabricated Al/Py devices suitable for measurement of nonlocal superconducting effects. We observe behavior characteristic of EC or CAR in the low temperature regime and nonlocal charge imbalance, arising as divergence in nonlocal differential resistance, close to  $T_c$ . In order to further investigate there results we have developed a simple numerical model of nonlocal processes in a lateral spin valve geometry device that is capable of qualitatively replicating the nonlocal effect trends with  $T$  and bias in experimental work here and in the literature, associated with the superconducting processes. The model is capable of quantitatively matching the nonlocal resistance from a real Al/Py device, using realistic parameters for the model variables. The single electron approach offers potential extension for shot noise calculation, of interest for recent cross correlation and entanglement studies. Although possibly inferior to a true analytical model, the numerical approach encompasses the key aspects of the physics of such a device and gives insight and the ability to replicate the typical local properties of a device and provides a simple way to derive important parameters such as  $\xi_0$  and  $\Lambda_Q$ .

#### V. ACKNOWLEDGEMENTS

This work was supported by a UK Engineering and Physical Sciences Research Council Advanced Research Fellowship EP/D072158/1.

\* email: pyjlw@leeds.ac.uk; web: <http://www.stoner.leeds.ac.uk>

<sup>1</sup> D. Beckmann, H. B. Weber, and H. v. Löhneysen, Physical Review Letters **93**, 197003 (2004).

<sup>2</sup> S. Russo, M. Kroug, T. M. Klapwijk, and A. F. Morpurgo, Physical Review Letters **95**, 027002 (2005).

<sup>3</sup> D. Beckmann and H. v. Löhneysen, Applied Physics A: Materials Science & Processing **89**, 603 (2007).

<sup>4</sup> J. Wei and V. Chandrasekhar, Nature Physics **6**, 494 (2010).

<sup>5</sup> P. Cadden-Zimansky, J. Wei, and V. Chandrasekhar, Nature Physics **5**, 393 (2009).

- <sup>6</sup> F. Hübler, J. C. Lemyre, D. Beckmann, and H. v. Löhneysen, *Physical Review B* **81**, 184524 (2010).
- <sup>7</sup> G. Deutscher and D. Feinberg, *Applied Physics Letters* **76**, 487 (2000).
- <sup>8</sup> G. E. Blonder, M. Tinkham, and T. M. Klapwijk, *Physical Review B* **25**, 4515 (1982).
- <sup>9</sup> T. Yamashita, S. Takahashi, and S. Maekawa, *Phys. Rev. B* **68**, 174504 (2003).
- <sup>10</sup> A. Brinkman and A. A. Golubov, *Physical Review B* **74**, 214512 (2006).
- <sup>11</sup> D. S. Golubev, M. S. Kalenkov, and A. D. Zaikin, *Physical Review Letters* **103**, 067006 (2009).
- <sup>12</sup> J. R. J. Soulen et al., *Journal of Applied Physics* **85**, 4589 (1999).
- <sup>13</sup> G. J. Strijkers, Y. Ji, F. Y. Yang, C. L. Chien, and J. M. Byers, *Physical Review B* **63**, 104510 (2001).
- <sup>14</sup> S. Russo, M. Kroug, T. M. Klapwijk, and A. F. Morpurgo, *Phys. Rev. Lett.* **95**, 027002 (2005).
- <sup>15</sup> J. Brauer, F. Hübler, M. Smetanin, D. Beckmann, and H. v. Löhneysen, *Physical Review B* **81**, 024515 (2010).
- <sup>16</sup> P. Cadden-Zimansky and V. Chandrasekhar, *Physical Review Letters* **97**, 237003 (2006).
- <sup>17</sup> P. Cadden-Zimansky, Z. Jiang, and V. Chandrasekhar, *New Journal of Physics* **9**, 116 (2007).
- <sup>18</sup> A. Kleine et al., *Nanotechnology* **21**, A264002 (2010).